

7. J. C. Clemente, L. K. Ursell, L. W. Parfrey, R. Knight, *Cell* **148**, 1258–1270 (2012).
8. R. L. Fisher, *J. Nutr.* **129** (suppl.), 252S–255S (1999).
9. C. Ubeda et al., *J. Clin. Invest.* **120**, 4332–4341 (2010).
10. I. Okayasu et al., *Gastroenterology* **98**, 694–702 (1990).
11. Materials and methods are available as supplementary materials on Science Online.
12. K. C. Fearon, D. J. Glass, D. C. Guttridge, *Cell Metab.* **16**, 153–166 (2012).
13. M. J. Tisdale, *Physiol. Rev.* **89**, 381–410 (2009).
14. L. Ovesen, L. Allingstrup, J. Hannibal, E. L. Mortensen, O. P. Hansen, *J. Clin. Oncol.* **11**, 2043–2049 (1993).
15. J. S. Ayres, N. J. Trinidad, R. E. Vance, *Nat. Med.* **18**, 799–806 (2012).
16. Z. A. Puthuchery et al., *JAMA* **310**, 1591–1600 (2013).
17. M. Barthel et al., *Infect. Immun.* **71**, 2839–2858 (2003).
18. S. Cohen et al., *J. Cell Biol.* **185**, 1083–1095 (2009).
19. S. C. Bodine et al., *Science* **294**, 1704–1708 (2001).
20. M. D. Gomes, S. H. Lecker, R. T. Jagoe, A. Navon, A. L. Goldberg, *Proc. Natl. Acad. Sci. U.S.A.* **98**, 14440–14445 (2001).
21. J. M. Sackeck, A. Ohtsuka, S. C. McLary, A. L. Goldberg, *Am. J. Physiol. Endocrinol. Metab.* **287**, E591–E601 (2004).
22. T. N. Stitt et al., *Mol. Cell* **14**, 395–403 (2004).
23. D. R. Clemmons, *Trends Endocrinol. Metab.* **20**, 349–356 (2009).
24. D. J. Chia, *Mol. Endocrinol.* **28**, 1012–1025 (2014).
25. N. Klöting et al., *Diabetes* **57**, 2074–2082 (2008).
26. J. von Moltke, J. S. Ayres, E. M. Kofoed, J. Chavarría-Smith, R. E. Vance, *Annu. Rev. Immunol.* **31**, 73–106 (2013).
27. J. Henao-Mejia, E. Elinav, C. A. Thaiss, R. A. Flavell, *Annu. Rev. Physiol.* **76**, 57–78 (2014).
28. N. Kayagaki et al., *Nature* **479**, 117–121 (2011).
29. J. S. Ayres, D. S. Schneider, *Annu. Rev. Immunol.* **30**, 271–294 (2012).
30. D. S. Schneider, J. S. Ayres, *Nat. Rev. Immunol.* **8**, 889–895 (2008).
31. R. Medzhitov, D. S. Schneider, M. P. Soares, *Science* **335**, 936–941 (2012).
32. I. I. Ivanov et al., *Cell* **139**, 485–498 (2009).
33. T. Ichinohe et al., *Proc. Natl. Acad. Sci. U.S.A.* **108**, 5354–5359 (2011).

ACKNOWLEDGMENTS

We thank R. Vance for mice and reagents; G. Barton and M. Koch for TLR4-ELAM NFκB reagents; M. Montminy and E. Wiater for use of the EchoMRI and MiSeq sequencer and technical assistance; S. Mazmanian, S. McBride, J. Sonnenburg, and S. Higginbottom for germ-free mice and advice; D. Monack and F. Re for *Salmonella* and *Burkholderia* strains; W. Fan and S. Bapat for reagents and help with muscle and fat anatomy and physiology; I. Verma for use of the BioRad Bio-Plex MAGPIX multiplex reader; D. Cook for technical assistance with Luminex assays; M. Ku and S. Heinz for advice and technical assistance with RNA-seq and metagenomics analyses; R. Shaw and P. Hollstein for Western blot reagents and advice; G. Van Gerpen, K. Kujawa, and M. Bouchard for administrative assistance with establishing our gnotobiotic facility; and D. Schneider and D. Green for helpful discussions and thoughtful comments on the manuscript. A special thanks to R. Lambertson for continuous support. This work was supported by NIH grant R01AI114929 (J.S.A.), the NOMIS Foundation, the Searle Scholar Foundation (J.S.A.), the Ray Thomas Edward Foundation (J.S.A.), NIH grants DK0577978 (R.M.E.) and CA014195, the Leona M. and Harry B. Helmsley Charitable Trust (2012-PG-MED002), the Samuel Waxman Cancer Research Foundation, and Ipsen/ Biomeasure. R.M.E. is an investigator of the Howard Hughes Medical Institute at the Salk Institute and March of Dimes Chair in Molecular and Developmental Biology. Data described in this paper can be found in the supplementary materials. The authors declare no conflicts of interest.

SUPPLEMENTARY MATERIALS

www.sciencemag.org/content/350/6260/558/suppl/DC1
Materials and Methods
Figs. S1 to S19
Tables S1 and S2
References (34–45)

25 May 2015; accepted 9 September 2015
10.1126/science.aac6468

VIROLOGY

Retroviruses use CD169-mediated trans-infection of permissive lymphocytes to establish infection

Xaver Sewald,^{1*†} Mark S. Ladinsky,^{2‡} Pradeep D. Uchil,^{1‡} Jagadish Beloor,³ Ruoxi Pi,¹ Christian Herrmann,¹ Nasim Motamedi,^{4†} Thomas T. Murooka,⁵ Michael A. Brehm,⁶ Dale L. Greiner,⁶ Leonard D. Shultz,⁷ Thorsten R. Mempel,⁵ Pamela J. Bjorkman,² Priti Kumar,^{3*} Walther Mothes^{1*}

Dendritic cells can capture and transfer retroviruses in vitro across synaptic cell-cell contacts to uninfected cells, a process called trans-infection. Whether trans-infection contributes to retroviral spread in vivo remains unknown. Here, we visualize how retroviruses disseminate in secondary lymphoid tissues of living mice. We demonstrate that murine leukemia virus (MLV) and human immunodeficiency virus (HIV) are first captured by sinus-lining macrophages. CD169/Siglec-1, an I-type lectin that recognizes gangliosides, captures the virus. MLV-laden macrophages then form long-lived synaptic contacts to trans-infect B-1 cells. Infected B-1 cells subsequently migrate into the lymph node to spread the infection through virological synapses. Robust infection in lymph nodes and spleen requires CD169, suggesting that a combination of fluid-based movement followed by CD169-dependent trans-infection can contribute to viral spread.

To understand how retroviruses disseminate in secondary lymphoid organs of living animals, we introduced fluorescently labeled murine leukemia virus (MLV) or human immunodeficiency (HIV) subcutaneously (s.c.) into footpads of anesthetized mice and monitored their arrival at the draining popliteal lymph node (pLN). MLV and HIV viruses accumulated at the floor of the subcapsular sinus (SCS), where the lymph node cortex faces the arriving lymphatic fluid (Fig. 1, A and B, and movies S1 and S2). MLV Gag-GFP (green fluorescent protein) viruses accumulated particularly at the SCS above B cell follicles and persisted for >6 hours, whereas beads conjugated with antibodies to the complement receptor 1/2 entered B cell follicles, as previously described (*1–3*) (Fig. 1A and fig. S1). The cell type responsible for MLV capture (GFP⁺) consisted mostly of CD169⁺ CD11b⁺ macrophages (~80%) (Fig. 1C and fig. S2) (*4, 5*). Within the pLN tissue, MLV Gag-GFP and HIV Gag-GFP were solely associated with CD169⁺ cells (Fig. 1D, figs. S3 and S4, and movie S3). No overlap between CD169 and CD3, CD19, or CD11c was

observed (fig. S5). When pLN macrophages were depleted, MLV capture was severely compromised (fig. S6).

These data indicate that MLV and HIV are captured in vivo at the pLN predominantly by CD169⁺ CD11b⁺ macrophages. The ability to capture and transmit HIV to permissive CD4⁺ T cells has previously been associated with dendritic cells (DCs), and two distinct mechanisms have been proposed (*6, 7*). First, by expressing C-type lectins such as DC-SIGN, DCs can capture HIV by recognizing the viral envelope glycoprotein (Env) (*7, 8*). Second, upon activation, DCs express the immunoglobulin (I)-type lectin CD169/Siglec-1 that can bind MLV and HIV through the recognition of sialyllactose on gangliosides that are embedded in the viral lipid membrane (*9–12*). To distinguish between both mechanisms, we first injected equal amounts of wild-type or mutant MLV lacking the viral envelope glycoprotein (ΔEnv) into the footpad of C57BL/6 mice, but observed no difference in virus capture at the draining pLN (Fig. 1E). In contrast, depletion of gangliosides in the retrovirus membrane (*13*) reduced MLV capture, suggesting a role for CD169/Siglec-1 (Fig. 1F). Indeed, a single injection of antibodies to CD169 before the administration of MLV and HIV impaired virus capture at the pLN SCS floor in C57BL/6 mice (Fig. 1, G and H, and fig. S7, A and B). MLV and HIV capture at pLNs were also significantly reduced in CD169 knockout mice (*Siglec1*^{−/−}) (*14*) compared to C57BL/6 mice (Fig. 1, I and J, and fig. S7C) (*15*). Blockade of the mouse DC-SIGN homolog SIGN-RI (*16*) had no effect on MLV capture in vivo (fig. S8).

CD169-expressing macrophages are frequently located at the borders between circulating fluids such as the lymph and blood, and lymphoid structures similar to those seen in LNs are also

¹Department of Microbial Pathogenesis, Yale University School of Medicine, New Haven, CT 06510, USA. ²Division of Biology and Biological Engineering, California Institute of Technology, Pasadena, CA 91125, USA. ³Department of Internal Medicine, Yale University School of Medicine, New Haven, CT 06510, USA. ⁴Department of Genetics, Yale University School of Medicine, New Haven, CT 06510, USA. ⁵Center for Immunology and Inflammatory Diseases, Massachusetts General Hospital, Harvard Medical School, Boston, MA 02114, USA. ⁶Program in Molecular Medicine, University of Massachusetts Medical School, Worcester, MA 01655, USA. ⁷The Jackson Laboratory, Bar Harbor, ME 04609, USA.

*Corresponding author. E-mail: sewald@mvp.uni-muenchen.de (X.S.); priti.kumar@yale.edu (P.K.); walther.mothes@yale.edu (W.M.) †Present address: Max von Pettenkofer-Institute, Ludwig-Maximilians-University Munich, Munich, Germany. ‡These authors contributed equally to this work.

observed in the marginal zone of the spleen (Fig. 1K) (17). Indeed, blood-derived MLV Gag-GFP particles were captured at the marginal zone by CD169⁺ macrophages (Fig. 1K and fig. S9). MLV capture at the spleen was significantly reduced by CD169-targeting antibodies, as well as

in *Siglec1*^{-/-} mice (Fig. 1, L and M). To similarly study early events during HIV infection, we used the BLT humanized mouse model, which exhibits good reconstitution of human macrophages and T cells (18). Fluorescently labeled HIV injected intravenously (i.v.) into humanized mice was as-

sociated with CD169⁺ CD11b⁺ macrophages in the engrafted CD45⁺ human cell population of the spleen (fig. S10). Blocking CD169 significantly reduced association between HIV and splenocytes (Fig. 1N and fig. S11). These data document that mouse and human CD169⁺ macrophages efficiently

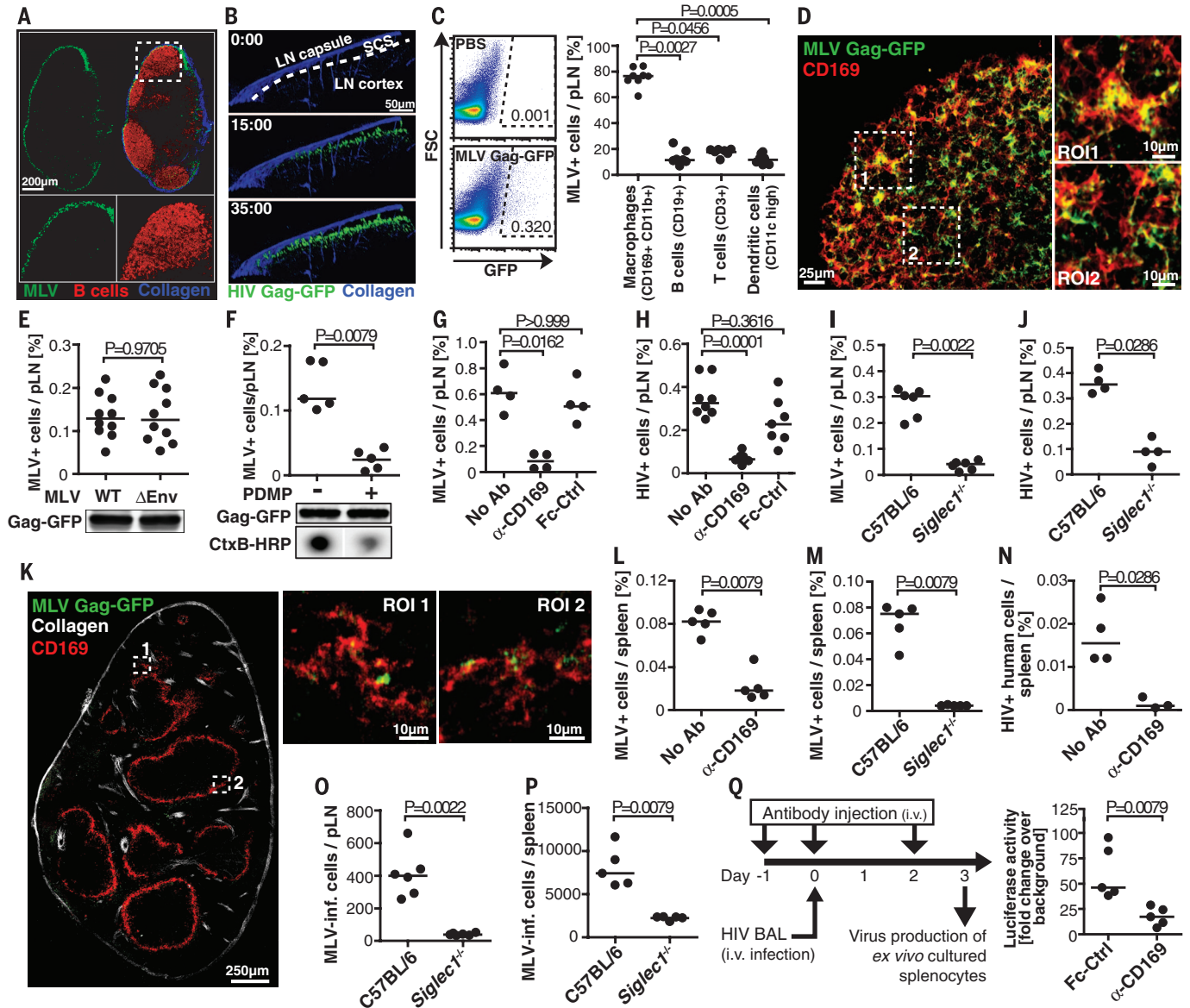


Fig. 1. MLV and HIV infection are facilitated by CD169/Siglec1-expressing macrophages.

(A) Immunohistochemistry of a pLN section 0.5 hours after s.c. injection of MLV Gag-GFP (green) into a C57BL/6 mouse. Red, B cells; blue, collagen. (B) Image sequence (movie S2) of HIV Gag-GFP (green) capture at pLN SCS floor (collagen, blue) after s.c. injection into C57BL/6 mouse. Time in minutes. (C) Quantification of MLV Gag-GFP capture at pLNs ($n = 7$ to 9) 1 hour after s.c. injection. MLV-binding (GFP⁺) cell types were identified by the indicated markers. FSC: front scatter; PBS: phosphate-buffered saline. (D) Image of MLV (green) capture by CD169-expressing macrophages (red) at the pLN SCS floor. CD169⁺ macrophages were stained by s.c. injection of CD169-CF568 antibodies. (E and F) Quantification of MLV capture at pLNs 1 hour after s.c. injection into C57BL/6 mice for wild-type (WT, $n = 10$), mutant (Δ Env, $n = 10$), or ganglioside-depleted MLV Gag-GFP [PDMP⁺ (1-phenyl-2-decanoylamino-3-morpholino-1-propanol), $n = 5$]. Total amounts of Gag-GFP were estimated by Western blotting and ganglioside depletion by cholera toxin

B-horseradish peroxidase (CtxB-HRP) staining. (G and H) MLV Gag-GFP ($n = 4$) and HIV Gag-GFP ($n = 7$ to 8) capture at the pLNs of C57BL/6 mice after injection of CD169 or control (Ctrl) antibodies. (I and J) MLV Gag-GFP ($n = 6$) and HIV Gag-GFP ($n = 4$) capture at the pLNs of C57BL/6 and *Siglec1*^{-/-} mice. (K) Immunohistochemistry of a spleen section 0.5 hours after i.v. injection of MLV Gag-GFP (green). Red, CD169; gray, collagen. (L and M) MLV Gag-GFP capture at the spleen after i.v. injection of CD169 antibodies ($n = 5$) or in *Siglec1*^{-/-} mice ($n = 5$). (N) HIV Gag-GFP capture at the spleen of humanized BLT mice in the absence or presence of CD169 antibodies ($n = 3$ to 4). (O and P) MLV-infected cells in pLNs ($n = 6$) and spleen ($n = 5$) of C57BL/6 and *Siglec1*^{-/-} mice 2 days after infection. (Q) HIV-infected splenocytes in humanized HSC mice injected with CD169 antibodies ($n = 5$). HIV production of ex vivo-cultured splenocytes was quantified with TZM-bl reporter cells. Median is shown in all cases. Kruskal-Wallis test followed by Dunn's posttest [(C), (G), and (H)]; Mann-Whitney test for (E), (F), and (I) to (Q).

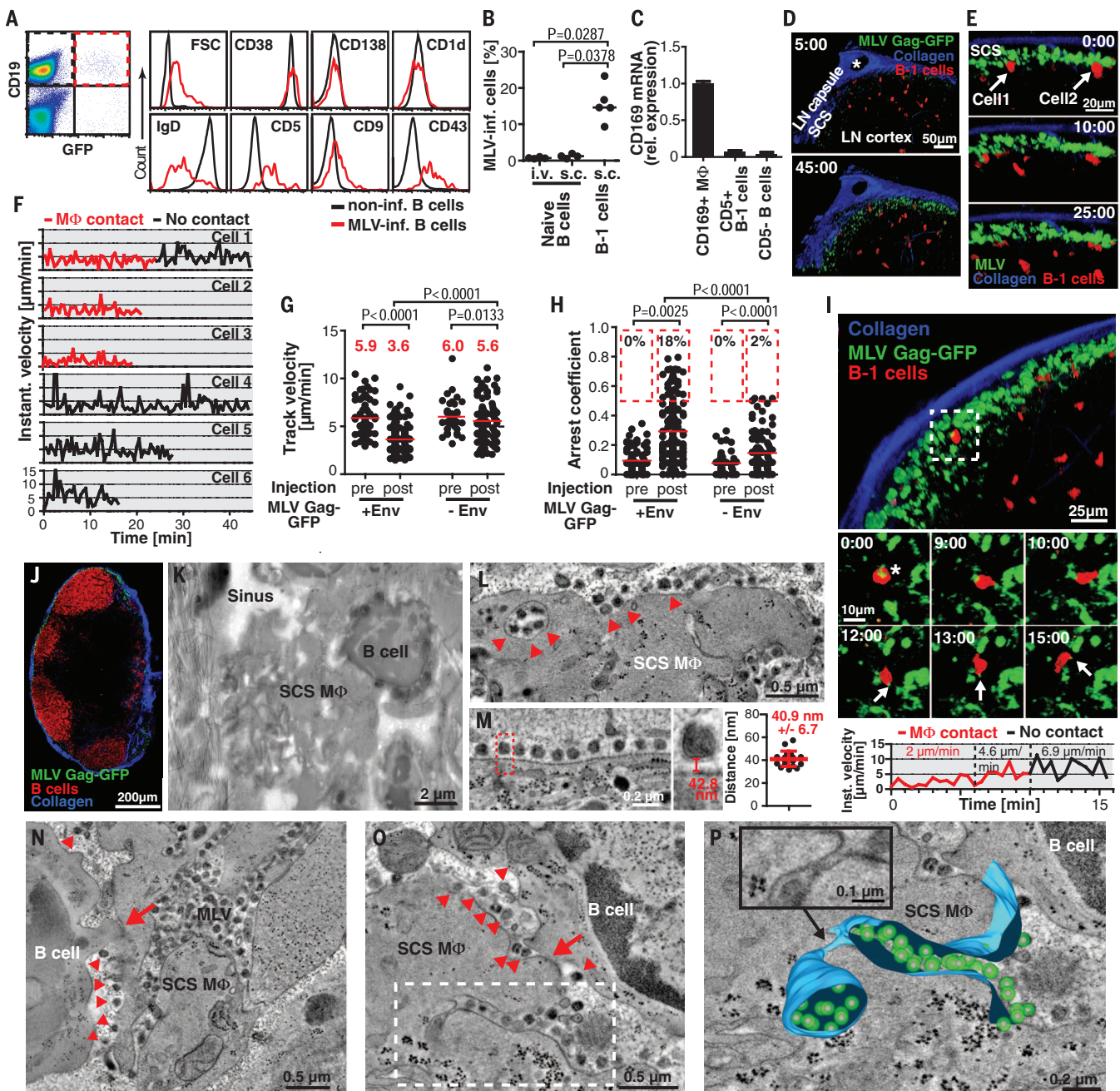


Fig. 2. MLV-laden CD169⁺ macrophages form Env-dependent contacts with B-1a cells for trans-infection. (A) Surface marker analysis of MLV-infected B cells in pLNs of C57BL/6 mice 2 days after s.c. infection. (B) Quantification of MLV-infected, adoptively transferred B-1 cells (s.c.) or naïve B cells (s.c., i.v.) ($n = 4$ to 5). (C) qPCR analysis of relative CD169 mRNA expression by pLN-derived CD5⁺ B-1a cells, CD5⁻ B cells, and CD169⁺ macrophages. Mean \pm SD shown. (D) Images (movie S5) of MLV (green) capture at pLN SCS floor containing RFP⁺ B-1 cells (red). Asterisk depicts afferent lymphatic vessel entry site. Blue, collagen. Time in minutes. (E) Image sequence (movie S6) of adoptively transferred RFP⁺ B-1 cells (red) and captured MLV Gag-GFP (green) at the pLN SCS floor. Arrows depict cells analyzed in (F). Time in minutes. (F) Instantaneous velocity of representative B-1 cell traces (from Fig. 2E and fig. S15A) in contact with MLV-laden macrophages (red line) or not (black line). (G and H) Track velocities and arrest coefficients of adoptively transferred RFP⁺ B-1 cells in pLNs before and after s.c. injection of MLV Gag-GFP carrying or lacking Env (+/-Env). Red lines and numbers in (G) are medians. Percentages in (H) are cell population that remained arrested (<2 $\mu\text{m}/\text{min}$) >50% of time. Data are from four (+Env, 159 tracks) and

three (-Env, 138 tracks) independent experiments. (I) Image sequence (movie S8) of MLV Gag-GFP (green) transfer to RFP⁺ B-1 cell (red) at pLN SCS floor, and B-1 cell instantaneous velocity over time. Asterisk, stable contact ($t = 0$ min); arrows, MLV Gag-GFP transfer to B-1 cell uropod ($t = 12$ to 15 min). (J and K) Immunohistochemistry and electron microscopy overview of a pLN 1 hour after s.c. injection of MLV. (L and M) Electron tomography of a MLV-laden macrophage at the pLN SCS floor and quantification of the cell-virus distance ($n = 19$). Arrowheads depict MLV particles at the surface and within the macrophage. (N to P) Electron tomographies and tomographic 3D reconstruction of synaptic contacts between MLV-laden macrophages and B cells at pLN SCS floor 1 hour after s.c. injection of MLV. Arrowheads depict MLV particles at contact site. Arrows show direct cell-cell contacts between macrophages and B cells (N and O). In the studied tissue sections, we observe 2.14 contacts per 1000 μm^2 (mean, SD = 1.2; $n = 9$). Inset in (P) shows continuity between the invagination and a virus-containing compartment. Kruskal-Wallis test followed by Dunn's posttest for (B); Wilcoxon matched-pairs signed rank test for (G) and (H) (pre- versus postinjection); Mann-Whitney test for (G) and (H) (+Env_{post} versus -Env_{post}).

capture blood- or lymph-borne retroviruses in spleen and lymph nodes.

The capture of MLV and HIV by CD169⁺ macrophages could be the first step toward the initiation of host immune responses against incoming viruses. Alternatively, retroviruses may have evolved to use this pathway to efficiently infect their hosts. To investigate these possibilities, we monitored MLV infection following s.c. virus injection in wild-type C57BL/6 and *Siglec1*^{-/-} mice. MLV infection was significantly reduced in pLNs and spleen of *Siglec1*^{-/-} mice, indicating that virus capture by CD169⁺ macrophages contributes to efficient infection (Fig. 1, O and P). Despite reduced MLV infection in *Siglec1*^{-/-} mice, neutralizing antibodies were produced with similar kinetics and were able to control the spread of MLV infection by day 7, as in wild-type C57BL/6 mice (fig. S12). HIV infection of splenocytes in humanized mice was also significantly lowered upon CD169 blockade (Fig. 1Q). Collectively, these results demonstrate that retrovirus capture via recognition of gangliosides within the virus mem-

brane by CD169/Siglec-1 expressed on macrophages promotes efficient retroviral infection in vivo.

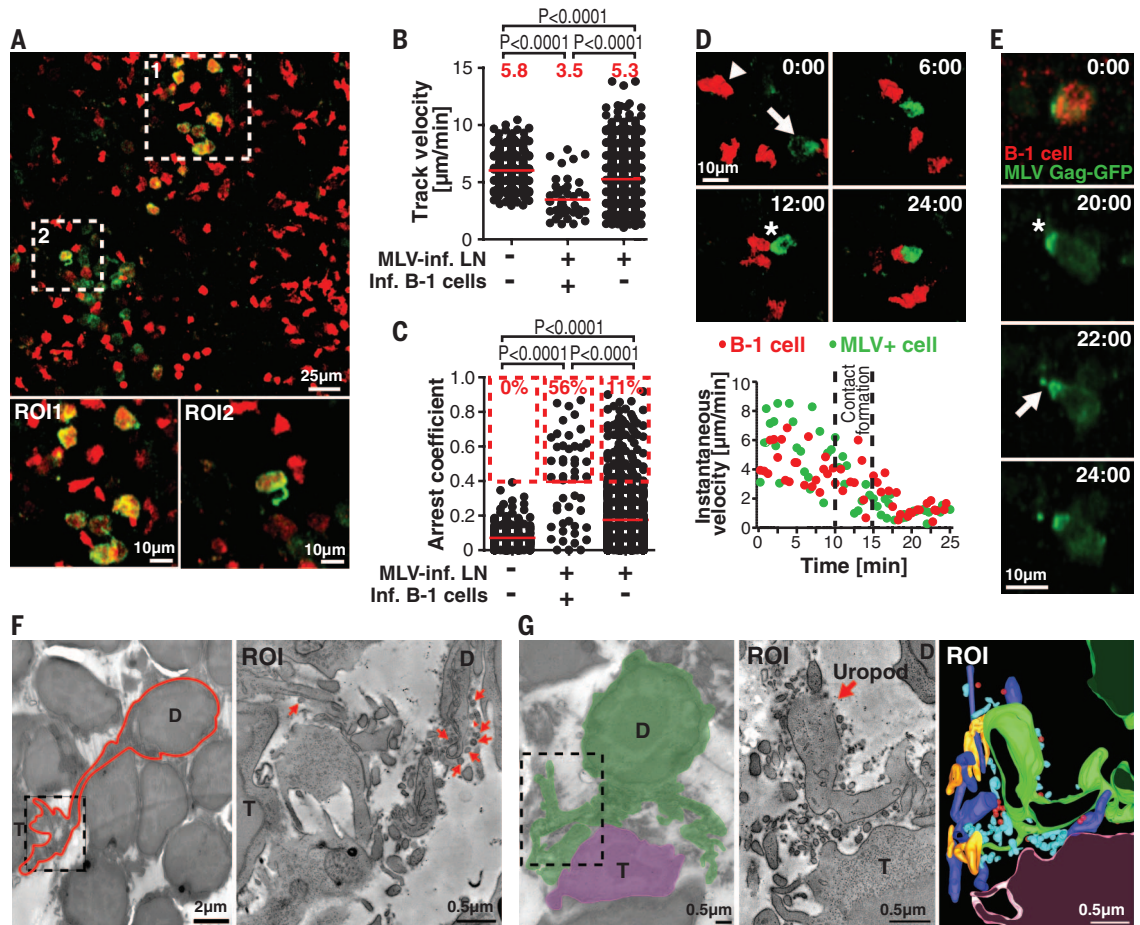
Interestingly, MLV does not infect CD169⁺ macrophages (19). Therefore, the likely role of CD169⁺ macrophages must be to trans-infect permissive lymphocytes. To visualize this, we first prepared naive B cells from mice expressing red fluorescent protein (RFP), adoptively transferred (i.v.) them into C57BL/6 mice, and infected the mice (s.c.) with MLV carrying a long-terminal repeat (LTR)-GFP reporter. Surprisingly, no RFP⁺ naive B cells were infected (fig. S13A and movie S4), yet MLV-infected cells were largely CD19⁺ B cells (19). We concluded that MLV must target a specific subset of B cells that is excluded during the preparation of naive B cells. We characterized these GFP⁺ MLV-infected cells as CD19⁺, CD43⁺, CD9⁺, CD5⁺, and IgD^{low}, which collectively defined them as B-1a cells (Fig. 2A) (20). B-1a cells are innate B cells, which secrete most of the circulating immunoglobulin M (IgM) (20). They undergo self-renewal

and thus are susceptible to MLV infection, owing to the virus's dependency on the cell cycle for nuclear entry (21). When we adoptively transferred (s.c.) RFP⁺ B-1 cells into C57BL/6 mice, incoming MLV specifically infected these cells but not naive B cells (Fig. 2B and fig. S13, B and C).

Having identified B-1a cells as target cells for MLV that lack CD169 expression (Fig. 2C and fig. S14), we attempted to directly visualize trans-infection events at the pLN SCS using two-photon laser scanning microscopy (2P-LSM). Upon arrival of MLV at the pLN, RFP⁺ B-1 cells were seen to sample the SCS, come in contact with MLV-laden SCS macrophages, and form long-lived synaptic contacts (Fig. 2, D to F; fig. S15A; and movies S5 to S7). B-1 cell migration velocity was significantly reduced upon contact with MLV-laden macrophages (Fig. 2F). This was also evident at the population level. B-1 cell track velocity decreased with a concomitant arrest coefficient increase after MLV injection (Fig. 2, G and H). In two instances (out of 159), following the disengagement from a synaptic contact with MLV-laden CD169⁺

Fig. 3. MLV-infected B-1 cells form stable virological synapses in infected pLNs.

(A) Image (from movie S11) of adoptively transferred RFP⁺ B-1 cells (red) in MLV Gag-GFP (green) infected pLN 2 days after infection. Regions of interest (ROIs) show Gag polarization (ROI1) and membranous protrusion (ROI2) of MLV-infected B-1 cells. (B and C) Track velocities and arrest coefficients of adoptively transferred RFP⁺ B-1 cells in noninfected and infected pLNs. Lines and numbers in (B) are medians. Percentage in (C) are static cell population that remained arrested (<2 $\mu\text{m}/\text{min}$) >60% of time. Data are from five independent experiments. Noninfected pLNs, 265 RFP⁺ B-1 cell tracks; MLV-infected pLNs, 48 MLV-infected and 361 noninfected B-1 cells tracks. Median is shown.



Kruskal-Wallis test followed by Dunn's posttest. (D) Image sequence (movie S12) and instantaneous velocity of an adoptively transferred RFP⁺ B-1 cell (red, arrowhead) forming stable contact with MLV-infected leukocyte (green, arrow). Asterisk ($t = 12$ min) depicts contact formation. (E) Image sequence (movie S12) of MLV Gag-GFP material release (arrow) from an infected B-1 cell at a virological synapse (asterisk). Time in minutes. (F and G) Electron tomography and 3D reconstruction of pLN 2 days after s.c. infection, showing

MLV-containing membranous material at contact site between the uropod of MLV-infected donor cells (D) and uninfected target cells (T). Arrowheads indicate viral particles at surface of infected cell. In the studied tissue sections, we observe 2.6 membrane protrusion contacts per 1000 μm^2 (mean, SD = 1.1; $n = 11$). A 3D reconstruction [(G), right panel]: green, donor cell uropod; pink, target cell; blue and gold, uropod-associated membranous tubules; red, MLV.

macrophages, B-1 cells carried Gag-GFP-positive viral material at the uropod (Fig. 2I, fig. S15B, and movies S8 and S9). Though rare, these events are consistent with the notion that synaptic contacts contribute to virus transfer from SCS macrophages to B-1 cells. Mechanistically, synaptic contacts resulted largely from the interaction between Env on viral particles, presented on macrophages, and its receptor mCAT-1 expressed in B-1 cells (Fig. 2, G and H).

To understand trans-infection events at the ultrastructural level, we analyzed pLNs by electron tomography 1 hour after s.c. injection of MLV (Fig. 2, J to P, and fig. S16). Beneath a layer of collagen fibers, macrophages formed a dense layer at the SCS floor, followed by B cells at the distal side (Fig. 2, J and K). MLV particles were observed at the plasma membrane and within vesicle-like structures of SCS macrophages (Fig. 2L and fig. S16). Three-dimensional (3D) reconstruction revealed that these virus-containing compartments were continuous with the plasma membrane (Fig. 2, O and P; fig. S16; and movie S10). MLV particles bound to the macrophage surface with an average distance of 40.9 ± 6.7 nm (Fig. 2M), matching the predicted length of the CD169 molecule (22). We observed zones of contacts between macrophages and B cells with MLV virions in the cell-cell interface (Fig. 2, N and O, and fig. S16). A large invagination carrying dozens of viruses was found to open toward the B cell (Fig. 2P). These data suggest that retroviruses residing in deep plasma membrane invaginations in macrophages and DCs (23–25) can be mobilized toward contact zones and likely contribute to viral dissemination in vivo.

We followed the fate of MLV-infected B-1 cells over the next 2 days. After initially being trapped at the SCS, owing to interaction with MLV-presenting macrophages, MLV-infected B-1 cells redistributed deeper into the pLN to localize beneath the SCS, as well as in the interfollicular area and B-T cell border (fig. S13, D and E). They largely avoided B cell follicles and the T cell zone (fig. S13H). Uninfected peritoneal B-1 cells localized similarly at steady state (fig. S13F). The location of some MLV-infected cells to the T cell zone is explained, as ecotropic MLV also infects some CD4⁺ T cells (fig. S13G) (19). In contrast, amphotropic MLV specifically targeted the B-1a cell population (fig. S13I). Thus, despite using different receptors, both ecotropic and amphotropic MLV targeted the susceptible B-1a cell population.

At day 2, MLV-infected B-1 cells were often observed immobilized in foci with other uninfected cells, including B-1 cells (Fig. 3A movie S11). In addition to infecting adoptively transferred RFP⁺ B-1 cells, ecotropic MLV (GFP⁺) also infected endogenous B-1a cells and some T cells (Fig. 2A and fig. S13I) (19). At higher resolution, MLV Gag-GFP was seen to accumulate at the cell-cell interface between infected and uninfected cells (Fig. 3A and movie S11). These data indicate that MLV forms virological synapses during native infection (19). The immobilization of MLV-infected B-1 cells due to the formation of viro-

logical synapses was also evident at the population level. Compared to the behavior of uninfected B-1 cells, MLV-infected B-1 cells migrated at reduced velocities and exhibited higher arrest coefficients (Fig. 3, B and C). Because infected cells formed virological synapses with uninfected RFP⁺ B-1 cells, the latter also exhibited reduced migration (Fig. 3, B and C). Thus, as seen 2 hours after infection in the SCS (Fig. 2, G and H), the spread of MLV infection 2 days after infection can be seen at the population level simply by tracking B-1 cells. Our ability to visualize infected donor cells (MLV Gag-GFP⁺) and some target cells (uninfected RFP⁺ B-1 cells) allowed us to capture individual stages of the biogenesis of virological synapses (Fig. 3D, fig. S17, and movie S12). The transfer of Gag-GFP⁺ material from infected cells to uninfected cells (Fig. 3E and movie S12) indicated that these contacts can be associated with the transfer of viral material. Because we cannot detect the transfer of single particles by 2P-LSM in vivo, these transmission events must include clusters of particles, as has been observed for HIV in vitro (26). To gain insight into the ultrastructural information of virological synapses, we used electron tomography (27). We identified numerous complex membranous protrusions to which many viral particles were localized. These protrusions were often long and formed contacts between both neighboring and distally located cells (Fig. 3, F and G; fig. S18; and movies S13 and S14). These membrane-rich protrusions originated from a donor cell and were as long as ~ 10 μ m (Fig. 3F)—a structure that was also occasionally observed by intravital imaging (Fig. 3A ROI 2, movie S11). These protrusions were rich in intracellular vesicles and mitochondria, indicating that they represent uropods. We have previously observed that MLV assembles and buds at the uropod in polarized B cells in vitro (28). Similarly, HIV has been observed to assemble and bud at the uropod of polarized T cells (29). Our data suggest a model in which uropods form virological synapses in vivo to mediate transfer of viruses via large membranous protrusions.

Our data support a model in which trans-infection and virological synapses can both contribute to the spread of viral infections in vivo. The data are also consistent with a role for cell-free virus in spreading, as an alternative mode to virus spread via migration of infected cells (30). CD169⁺ macrophages are located at the interface between fluid phases such as the lymph, blood, and lymphoid tissue. They can concentrate cell-free viruses from the fluid phase to deliver them efficiently to permissive lymphocytes for infection. This model (fig. S19) suggests that viruses can disseminate by a combination of cell-free and cell-to-cell transmission, whereby viruses can use fluid flow-based dissemination over long distances and then cross the bottleneck at lymphoid tissue interfaces by exploiting the extraordinary ability of CD169⁺ macrophages to capture cell-free virus and trans-infect permissive lymphocytes. The relevance of this model for HIV transmission and its potential for therapeutic intervention will require further in vivo testing.

REFERENCES AND NOTES

1. T. G. Phan, I. Grigorova, T. Okada, J. G. Cyster, *Nat. Immunol.* **8**, 992–1000 (2007).
2. T. G. Phan, J. A. Green, E. E. Gray, Y. Xu, J. G. Cyster, *Nat. Immunol.* **10**, 786–793 (2009).
3. Y. R. Carrasco, F. D. Batista, *Immunity* **27**, 160–171 (2007).
4. As pLN sample preparation leads to cross-contamination, particularly of CD169⁺ macrophages markers on to other cells (5), we flanked all flow cytometry data with immune histochemistry.
5. E. E. Gray, S. Friend, K. Suzuki, T. G. Phan, J. G. Cyster, *PLoS ONE* **7**, e38258 (2012).
6. P. U. Cameron *et al.*, *Science* **257**, 383–387 (1992).
7. T. B. Geijtenbeek *et al.*, *Cell* **100**, 587–597 (2000).
8. S. G. Turville *et al.*, *Nat. Immunol.* **3**, 975–983 (2002).
9. N. Izquierdo-Useros *et al.*, *PLoS Biol.* **10**, e1001315 (2012).
10. W. B. Puryear, X. Yu, N. P. Ramirez, B. M. Reinhard, S. Gummuru, *Proc. Natl. Acad. Sci. U.S.A.* **109**, 7475–7480 (2012).
11. W. B. Puryear *et al.*, *PLoS Pathog.* **9**, e1003291 (2013).
12. N. Izquierdo-Useros *et al.*, *PLoS Biol.* **10**, e1001448 (2012).
13. Materials and Methods are available as supplementary materials on Science Online.
14. C. Oetke, M. C. Vinson, C. Jones, P. R. Crocker, *Mol. Cell. Biol.* **26**, 1549–1557 (2006).
15. MLV Gag-GFP produced in mouse embryonic fibroblasts rather than human HEK293 cells, was similarly captured at the pLN in a CD169-dependent manner (fig. S7D). Future in vivo studies should address the CD169-dependence for endogenously produced MLV.
16. Y. S. Kang *et al.*, *Proc. Natl. Acad. Sci. U.S.A.* **101**, 215–220 (2004).
17. L. Martinez-Pomares, S. Gordon, *Trends Immunol.* **33**, 66–70 (2012).
18. M. W. Melkus *et al.*, *Nat. Med.* **12**, 1316–1322 (2006).
19. X. Sewald, D. G. Gonzalez, A. M. Haberman, W. Mothes, *Nat. Commun.* **3**, 1320 (2012).
20. N. Baumgarth, *Nat. Rev. Immunol.* **11**, 34–46 (2011).
21. T. Roe, T. C. Reynolds, G. Yu, P. O. Brown, *EMBO J.* **12**, 2099–2108 (1993).
22. P. R. Crocker *et al.*, *EMBO J.* **10**, 1661–1669 (1991).
23. K. Goussset *et al.*, *PLoS Pathog.* **4**, e1000015 (2008).
24. A. E. Bennett *et al.*, *PLoS Pathog.* **5**, e1000591 (2009).
25. R. L. Felts *et al.*, *Proc. Natl. Acad. Sci. U.S.A.* **107**, 13336–13341 (2010).
26. W. Hübner *et al.*, *Science* **323**, 1743–1747 (2009).
27. M. S. Ladinsky *et al.*, *PLoS Pathog.* **10**, e1003899 (2014).
28. F. Li, X. Sewald, J. Jin, N. M. Sherer, W. Mothes, *J. Virol.* **88**, 10541–10555 (2014).
29. G. N. Llewellyn, I. B. Hogue, J. R. Grover, A. Ono, *PLoS Pathog.* **6**, e1001167 (2010).
30. T. T. Murooka *et al.*, *Nature* **490**, 283–287 (2012).

ACKNOWLEDGMENTS

We thank J. Grover, J. Ventura, and K. Haugh for critical reading of the manuscript; P. Van Ness for advice with statistical analyses; and P. Crocker, D. Gonzalez, and A. Haberman for *Siglec*^{−/−} mice and DsRed mice, respectively. *Siglec*^{−/−} mice are available under a materials transfer agreement with P. Crocker (University of Dundee, UK). This work was supported by the NIH grants R01 CA098727 and S10 RR026697 to W.M.; P50GM082545 to P.J.B. and W.M.; R01 AI097052, R01 DA036298, and P01 AI078897 to T.R.M.; R01 AI112443 to P.K.; Flow Cytometry Shared Resource of the Yale Cancer Center P30 CA016359 and the Leopoldina Fellowship LPDS2009-21 to X.S.; and a fellowship from the China Scholarship Council–Yale World Scholars to R.P. D.L.G. and M.A.B. are consultants for and receive grants from The Jackson Laboratory.

SUPPLEMENTARY MATERIALS

www.sciencemag.org/content/350/6260/563/suppl/DC1
Materials and Methods
Figs. S1 to S19
Movies S1 to S14
References (31–38)

2 April 2015; accepted 17 September 2015
Published online 1 October 2015
10.1126/science.aab2749

This copy is for your personal, non-commercial use only.

If you wish to distribute this article to others, you can order high-quality copies for your colleagues, clients, or customers by [clicking here](#).

Permission to republish or repurpose articles or portions of articles can be obtained by following the guidelines [here](#).

The following resources related to this article are available online at www.sciencemag.org (this information is current as of October 29, 2015):

Updated information and services, including high-resolution figures, can be found in the online version of this article at:

<http://www.sciencemag.org/content/350/6260/563.full.html>

Supporting Online Material can be found at:

<http://www.sciencemag.org/content/suppl/2015/09/30/science.aab2749.DC1.html>

A list of selected additional articles on the Science Web sites **related to this article** can be found at:

<http://www.sciencemag.org/content/350/6260/563.full.html#related>

This article **cites 35 articles**, 10 of which can be accessed free:

<http://www.sciencemag.org/content/350/6260/563.full.html#ref-list-1>